Stopped-Flow Kinetic Analysis of the Ligand-Induced Coil−Helix Transition in Glutathione *S*-Transferase A1-1: Evidence for a Persistent Denatured State†

Brenda S. Nieslanik, Michael J. Dabrowski, Robert P. Lyon, and William M. Atkins*

Department of Medicinal Chemistry, Box 357610, University of Washington, Seattle, Washington 98195-7610

Received December 10, 1998; Revised Manuscript Received February 17, 1999

ABSTRACT: Structural studies have suggested that the glutathione *S*-transferase (GST) A1-1 isozyme contains a dynamic C-terminus which undergoes a ligand-dependent disorder−order transition and sequesters substrates within the active site. Here, the contribution of the C-terminus to the kinetics and thermodynamics of ligand binding and dissociation has been determined. Steady-state turnover rates of the wild type (WT) and a C-terminal truncated (Δ209−222) rGST A1-1 with ethacrynic acid (EA) were measured in the presence of variable concentrations of viscogen. The results indicate that a physical step involving segmental protein motion is at least partially rate limiting at temperatures between 10 and 40 °C for WT. Dissociation rates of the glutathione−ethacrynic acid product conjugate (GS−EA), determined by stopped-flow fluorescence, correspond to the steady-state turnover rates. In contrast, the chemical step governs the turnover reaction by Δ209−222, suggesting that the slow rate of product release for WT is controlled by the dynamics of the C-terminal coil−helix transition. In addition, the association reaction of WT rGST A1-1 with GS−EA established that the binding was biphasic and included ligand docking followed by slow isomerization of the enzyme−ligand complex. In contrast, binding of GS−EA to Δ209−222 was a monophasic, bimolecular reaction. These results indicate that the binding of GS−EA to WT rGST A1-1 proceeds via an induced fit mechanism, with a slow conformational step that corresponds to the coil−helix transition. However, the biphasic dissociation kinetics for the wild type, and the recovered kinetic parameters, suggest that a significant fraction of the [GST·GS−EA] complex (∼15%) retains a persistent disordered state at equilibrium.

The glutathione *S*-transferases (GSTs)[1] are a family of dimeric enzymes which catalyze the conjugation of glutathione (GSH) to various electrophiles. One function of the enzymes, in vivo, is to detoxify carcinogens, anti-cancer drugs, pesticides, and reactive products generated under oxidative stress, such as α−β unsaturated carbonyls, quinones, and hydroperoxides (*1*−*3*). The conjugation of GSH with a foreign compound generally results in the formation of a nontoxic product that can be readily eliminated (*4*). The mammalian cytosolic GSTs comprise six gene classes which can be distinguished on the basis of structure and substrate specificity: alpha (A), mu (M), pi (P), theta (T), sigma (S), and kappa (K) (*5*−*7*). The GSTs provide an active site environment that favors the deprotonation of GSH to the nucleophilic thiolate (GS^-), which is $\sim 10^9$ times more reactive toward electrophiles than the protonated thiol (*8*). Each GST contains a conserved tyrosine or serine residue at the active site which hydrogen bonds to and stabilizes the thiolate ($OH\cdots{}^-SG$), thereby contributing to a reduction in the pK_a of the GSH from 9.3 to 6.3−7.4 (*9*−*14*). Although the GSTs share this common catalytic mechanism, X-ray structures indicate differences in the active sites of individual isoforms, particularly in the substrate binding region (H-site), where substrate selectivity is conferred (*15*).

A unique characteristic of the A-class GSTs is the C-terminus (residues 208−222), which undergoes a ligand-dependent coil−helix transition that appears to trap the bound ligand in the H-site. In the absence of ligand, however, the C-terminus is not observed crystallographically, presumably because it is highly dynamic or statically disordered (Figure 1; *16*, *17*). Here, we use the term "coil" to indicate a segment that is crystallographically invisible, although it is unlikely that this segment is a true random coil (the C-terminus may be a highly delocalized helix in the absence of ligand, but available data do not clarify the situation). Previous studies with rGST A1-1 indicate that mutations at Phe-220 within the helix significantly affect both the pK_a of the enzyme-bound GSH and steady-state turnover rates with the electrophilic substrates, CDNB, ethacrynic acid, and cumene hydroperoxide (*11*, *18*). These results, and studies with the A2-2 isozyme, suggest that the C-terminal coil−helix transition plays a key role in the function of the A-class enzymes (*19*).

To gain additional insight into the mechanistic details of the catalytic cycle, and the molecular mechanism by which the C-terminus affects substrate binding, product release, or

† This work was supported by the National Institutes of Health (Grants GM51210 and GM7750) and Merck Research Labs (Rahway, NJ).

* To whom correspondence should be addressed. Phone: (206) 685-0379. Fax: (206) 685-3252. E-mail: winky@u.washington.edu.

[1] Abbreviations: CDNB, 1-chloro-2,4-dinitrobenzene; EA, ethacrynic acid; GS−EA, Michael adduct of EA and glutathione; GSH, glutathione; rGST A1-1, GST A1-1 isoform isolated from rat; hGST A1-1, GST A1-1 isoform isolated from human; MES, 2-(*N*-morpholino)ethanesulfonic acid; WT, wild-type rGST A1-1; Δ209−222, rGST A1-1 C-terminal truncation mutant.

10.1021/bi9829130 CCC: $18.00
Published on Web 05/06/1999

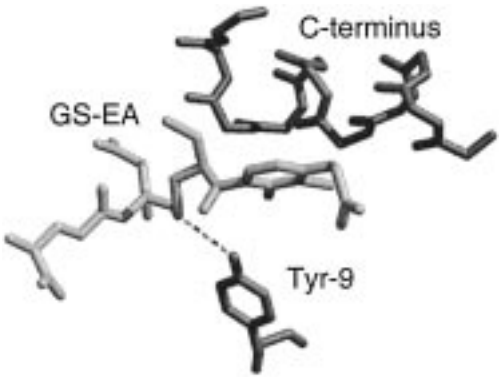

FIGURE 1: Active site structure of hGST A1-1 illustrating the position of bound GS−EA, the C-terminal helix (residues 208−222), and catalytic Tyr-9. The hydrogen bond between Tyr-9 and the sulfur of GS−EA is shown by the dashed line. The structure is adapted from Cameron et al. (*16*).

an intermediate step of the conjugation reaction, we have performed a steady-state and a pre-steady-state kinetic analysis with wild-type rGST A1-1 (WT), and a C-terminally truncated (Δ209−222) rGST A1-1, similar to the A2-2 truncation mutant studied previously (*19*). Although the importance of the C-terminal helix in the ligand binding in the A-class GSTs has been suggested, a detailed kinetic or thermodynamic analysis for this coil−helix transition has not been reported. Therefore, steady-state reaction rates for the reaction of rGST A1-1 with the commonly used in vitro substrate, ethacrynic acid (EA), were measured in the presence of viscogen to examine the contribution of segmental protein motion to turnover rates and to identify the rate-limiting step of the conjugation reaction from 10 to 50 °C. In addition, we have studied the kinetics of the binding and dissociation of the glutathione−ethacrynic acid product conjugate (GS−EA) to WT and Δ209−222 rGST A1-1 by stopped-flow fluorescence to relate the kinetic mechanism of ligand binding to the transition of the C-terminus from its disordered (unbound) to ordered (ligand bound) state. Because the interactions between ethacrynic acid and the GSTs have been studied extensively and X-ray structures are available for hGST A1-1 complexed with GS−EA and EA, these ligands are ideal probes for correlating the kinetics of binding to structural transitions (*16*, *17*, *20*−*23*). The experiments described herein allow for the unambiguous assignment of a spectroscopically defined rate constant to a structural transition of the C-terminus. Specifically, our results indicate that binding of GS−EA to rGST A1-1 proceeds via an induced fit mechanism, with a slow conformational step that coincides with the coil−helix transition. In addition, the K_{eq} for this transition indicates that a substantial amount of the [GST·GS−EA] complex retains a disordered C-terminus at equilibrium.

MATERIALS AND METHODS

Chemicals. GSH, EA, CDNB, and MES were obtained from Sigma (St. Louis, MO). GS−EA was synthesized according to the method of Ploeman et al. (*24*). Mass spectrometry and ^{1}H NMR were used to confirm the purity of the GS−EA product conjugate, and spectra agreed well with the predicted structure.

Protein Expression, Purification, and Activity. The expression and purification of the WT rGST A1-1 protein have been described previously (*25*). The truncation mutant Δ209−222 was constructed by PCR-based amplification of a fragment spanning the *Bgl*II and *Sal*I restriction sites contained in the linearized pKKGTB34 plasmid. The plasmid pKKGTB has been described previously (*26*). The sequence of the oligonucleotide primer encoding the amino acid truncation was 5′-GCAGGGGCCGTCGACCTACATG-GCTGGCTTTCTCTG-3′ and spanned the *Sal*I site. The PCR product was digested with *Sal*I and *Bgl*II and subcloned into pKKGTB34. Conditions for the PCR were 10 mM $(NH_4)_2SO_4$, 20 mM Tris (pH 8.3), 3 mM $MgSO_4$, each dNTP at 200 μM, 0.1% Trition X-100, 10 ng of linearized template, and 100 pmol of each primer in a final volume of 100 μL, with 1 unit of Vent polymerase (New England Biolabs). The cycle profile was 94 °C for 1 min, 65 °C for 2 min, and 72 °C for 2 min for 25 cycles followed by 10 min at 72 °C. The truncation mutant was verified by DNA sequencing. The enzymatic activities of WT and Δ209−222 were determined by the CDNB assay (*27*).

Steady-State Activity and Viscosity Effects. All reaction solutions were diluted into 100 mM MES buffer (pH 6.5) containing 1 mM EDTA. UV/vis absorbance spectra were recorded on a Cary 3E UV/vis spectrophotometer. Steady-state enzyme activity with ethacrynic acid (EA) was monitored at 270 nm in reaction mixtures containing 0.25 mM GSH and 0.1−0.6 mM EA (*27*). The microviscosity of the buffer was varied by the addition of 0−30% (w/w) sucrose, and rates of enzyme turnover with EA were obtained from 10 to 50 °C, as discussed above. The relative viscosity ($\eta/\eta°$) of each buffer was measured with an Ostwald viscometer at each reaction temperature and ranged from 1.0 to 2.9.

GST Binding and Dissociation Kinetics. Binding and dissociation experiments were performed with a BioLogic SFM4/QFM stopped-flow fluorimeter with a dead time of 2.3 ms. The fluorescence cuvette and all reaction solutions were maintained at constant temperature (10−40 °C) using a circulating water bath. Fluorescence measurements were taken at an excitation wavelength of 280 nm using a 309 nm cutoff filter, with signal sampling every 0.1−1 ms. The rate of binding was measured by the decrease in protein fluorescence after mixing an equal volume of 2 μM GST and 10−100 μM GS−EA. At each GS−EA concentration, 20−30 experiments were performed sequentially, and the kinetic traces were averaged. WT kinetic data were analyzed with the Bio-Kine analysis software and fit to a biexponential equation (eq 1) at temperatures of ≤20 °C:

$$f(x) = a_1 \exp^{-k_{obs1}t} + a_2 \exp^{-k_{obs2}t} + C \qquad (1)$$

where a_1 and a_2 are the amplitudes of two exponentials with rate constants k_{obs1} and k_{obs2}, respectively, t is time in seconds, and C is the offset. Above 20 °C, a single-exponential equation best described the approach to equilibrium for WT A1-1. For Δ209−222, the approach to equilibrium fit to a single-exponential equation at all temperatures that were studied. Association rates, k_1 and k_2, for the binding reaction were determined separately from plots of k_{obs1} and k_{obs2} versus GS−EA concentration.

Dissociation of product from the [GS−EA·GST] complex was followed by the increase in fluorescence after rapidly mixing 2 μM complex with an equal volume of 1 or 2 mM

Table 1: Comparison of Steady-State Turnover Rates for EA and Dissociation Rates of GS−EA with WT and Δ209−222 rGST A1-1

	WT					Δ209−222		
	k_{cat}[a] (s^{-1})	Amp_{-1}[b]	k_{-1} (s^{-1})	Amp_{-2}	k_{-2} (s^{-1})	k_{cat}[a] (s^{-1})	Amp_{-1}	k_{-1} (s^{-1})
10 °C	0.823 ± 0.021	0.00610	10.8	0.0225	0.748	0.240 ± 0.104	0.0263	20.4
25 °C	2.58 ± 0.25	0.00329	37.9	0.0246	1.77	0.435 ± 0.086	0.0138	48.7
40 °C	3.44 ± 0.70				11.8	0.837 ± 0.138		
50 °C	6.02 ± 0.99							

[a] k_{cat} is the observed steady-state turnover rate. [b] Throughout the text and tables, amplitude 1 (Amp_1), amplitude −1 (Amp_{-1}), amplitude 2 (Amp_2), and amplitude −2 (Amp_{-2}) refer to the magnitude of the pre-exponential terms for rate constants k_1, k_{-1}, k_2, and k_2, respectively. From triplicate measurements, where each was an average of 30 kinetic runs, the standard deviation in the rate constants was less than ±0.50 for k_1, less than ±0.80 for k_{-1}, less than ±0.70 for k_2, and less than ±0.25 for k_{-2}.

glutathionesulfonic acid (GSO_3^-) at temperatures ranging from 10 to 40 °C. Addition of GSO_3^- alone caused no change in the fluorescence intensity. Identical rate constants for dissociation of GS−EA were obtained at either GSO_3^- concentration, indicating that it binds sufficiently fast to trap the GST without GS−EA being bound. Dissociation rate constants for GS−EA with WT, k_{-1} and k_{-2}, were obtained directly from the biexponential equation (eq 1) at temperatures of ≤30 °C, and from a single-exponential decay at 40 °C. The dissociation rate constant, k_{-1}, for Δ209−222 was obtained from a fit to the single-exponential decay at all temperatures that were studied.

K_d Determination. The equilibrium dissociation constants (K_d) of GS−EA for dissociation from WT and Δ209−222 rGST A1-1 were determined from the change in intrinsic fluorescence as described for the kinetic experiments, measured on an SLM-Aminco 8100 spectrofluorimeter. In titration experiments, 0.03−500 μM GS−EA was added to an equal volume of 2 μM GST and the reduction in equilibrium fluorescence was monitored. The maximal fluorescence intensity was measured at 325 and 328 nm for the WT and Δ209−222 apoenzymes, and the emission maxima shifted to 330−331 nm upon binding of saturating GS−EA. K_d values were determined with eq 2 with the program Enzfitter:

$$[GS-EA]_{bound} = (\text{binding capacity} \times [GS-EA]_{free})/(K_d + [GS-EA]_{free}) \quad (2)$$

K_d values were also calculated from the ratio of the experimentally determined binding and dissociation rate constants, as shown in the Results.

RESULTS

Viscosity Effects on Turnover Rates. Ideally, binding and dissociation rates must be related to the overall rate of substrate turnover. However, because the individual steps of enzyme turnover may be differentially sensitive to temperature, it is often difficult to relate binding and dissociation kinetics determined at a single temperature to turnover rates measured at a different temperature. Steady-state experiments were therefore performed with WT rGST A1-1 and EA at temperstures ranging from 10 to 50 °C. Turnover rates (V_{max}) with EA ranged from 0.823 s^{-1} at 10 °C to 6.02 s^{-1} at 50 °C (Table 1). To characterize the rate-limiting step of the reaction, 0−30% (w/w) sucrose was added to the reaction mixtures and enzyme activity was measured. According to the Stokes−Einstein relationship, a diffusion-controlled rate constant is inversely related to the viscosity of the reaction solution (*28*). Therefore, the $k_{cat}°$ observed at a reference viscosity equal to that of buffer, $\eta°$, will be related to the k_{cat} observed at a higher viscosity, η, by eq 3:

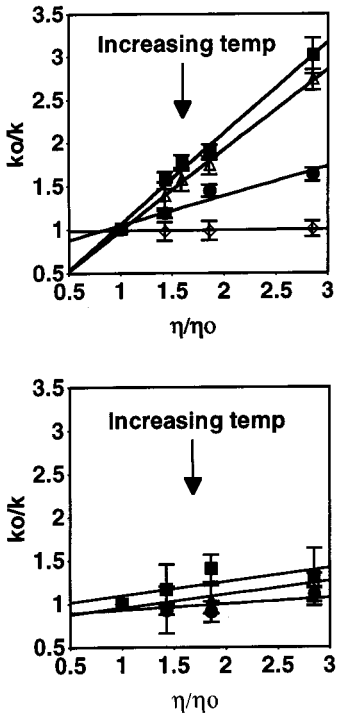

FIGURE 2: Dependence of the relative steady-state turnover rates $k_{cat}°/k_{cat}$ on the relative viscosity $\eta/\eta°$ for EA with WT (top) and Δ209−222 (bottom). (Top) Slopes of the viscosity dependence at each temperature for WT, derived from the least-squares fit to the experimental data, are 1.06 ± 0.12, 0.93 ± 0.13, 0.34 ± 0.07, and 0.008 ± 0.01 at 10 (■), 25 (△), 40 (●), and 50 °C (◇), respectively. (Bottom) Slopes of the viscosity dependence at each temperature for Δ209−222 are 0.16 ± 0.19, 0.15 ± 0.08, and 0.07 ± 0.04 at 10 (■), 25 (△), and 40 °C (●), respectively. The wild type exhibits a transition from a rate-limiting physical step to a rate-limiting chemical step between 10 and 40 °C. The Δ209−222 mutant has a rate-limiting chemical step at all temperatures in this range.

$$k_{cat}°/k_{cat} = \eta/\eta° \quad (3)$$

where k_{cat} is defined as the overall turnover rate. A plot of $k_{cat}°/k_{cat}$ versus $\eta/\eta°$ will have a slope of 1.0 when a physical step of the reaction (such as product binding or release) is rate-limiting, or a slope approaching zero if the chemical reaction step is rate-limiting.

The influence of viscogen on the steady-state reaction rates of WT rGST A1-1 with EA illustrates that the rate-limiting step changes as the reaction temperature is increased from 10 to 50 °C (Figure 2, top). At 10 and 25 °C, the slope of the linear regression line is approximately 1.0, suggesting

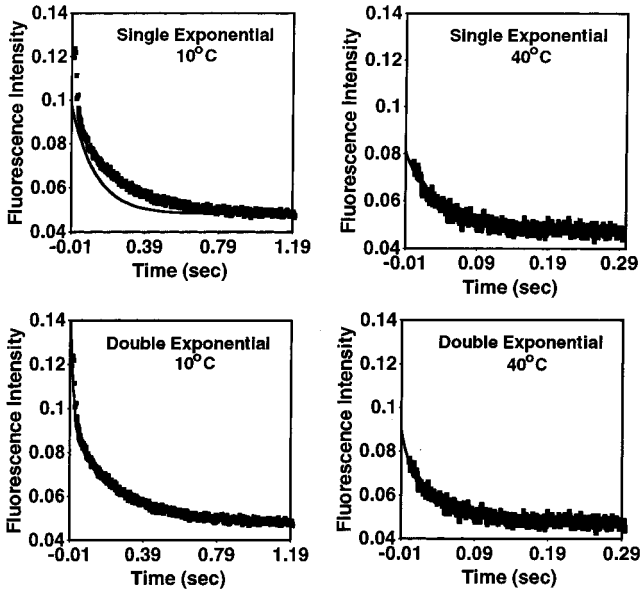

FIGURE 3: Representative data for the binding of 10 μM GS−EA to 1 μM WT rGST A1-1 at 10 (left) and 40 °C (right). (Top left) The single-exponential fit to the fluorescence data at 10 °C is shown ($R^2 = 0.76$). (Bottom left) The double-exponential fit to the raw data at 10 °C is shown ($R^2 = 0.99$). (Top right) The single-exponential fit to the raw data at 40 °C is shown ($R^2 = 0.92$). (Bottom right) The double exponential fit to the fluorescence data at 40 °C is shown ($R^2 = 0.93$). At lower temperatures, the association reaction is biphasic.

that a physical reaction step is rate-limiting. In contrast, at 50 °C, a slope of zero indicates that the chemical step of the reaction is rate-limiting. The reaction is partially limited by both the chemical and a physical step at 40 °C.

To determine whether the C-terminus contributes to the rate-limiting step of the reaction, steady-state kinetic parameters for the C-terminal truncation mutant, Δ209−222, and the substrate EA were also measured. As has been shown previously with other substrates such as CDNB and cumene hydroperoxide, turnover rates for EA were much slower for the C-terminally truncated mutant than for WT (Table 1; *19*). In addition, in contrast to the case with WT, viscosity had virtually no affect on k_{cat} at all of the temperatures that were studied (Figure 2, bottom). These results demonstrate not only that the rate-limiting step for WT A1-1 switches from a physical to the chemical step as the temperature is raised but also that the C-terminus plays a major role in determining the rate-limiting step of the conjugation reaction.

WT Binding and Dissociation Kinetics. Stopped-flow fluorescence experiments were performed to measure the rate of binding of GS−EA to WT rGST A1-1. Previous studies indicate that the binding of the H-site ligand, *S*-hexylglutathione, increases the fluorescence of the single tryptophan in the enzyme (*29*). However, a decrease in the intrinsic GST fluorescence was monitored after the rapid mixing of 10−100 μM GS−EA with 2 μM GST at temperatures ranging from 10 to 40 °C. Apparently, the net change in protein fluorescence is dependent on the H-site ligand. For GS−EA, a double-exponential decay was required to fit the raw data at temperatures of ≤20 °C, while a single-exponential decay adequately described the approach to equilibrium above 20 °C (Figure 3). Presumably at 40 °C, the fast phase of the reaction observed from 10 to 20 °C is complete within the dead time of the instrument. Therefore, the approach to equilibrium appears to be monophasic rather than biphasic, at the higher temperature. The addition of a third relaxation time did not improve the statistical fits. k_{obs1} and k_{obs2} were plotted separately versus GS−EA concentration ([GS−EA]) to determine the association rate constants, k_1 and k_2, for the fast and slow relaxation processes at temperatures of ≤20 °C. Plots of k_{obs1} versus [GS−EA] were linear, while a hyperbolic dependence of k_{obs2} versus [GS−EA] was observed, which leveled off at high substrate concentrations (Figure 4, left and middle). At temperatures at which a single-exponential decay was monitored, a hyperbolic dependence between k_{obs} and [GS−EA] was observed (Figure 4, right). Together, these results indicate the existence of a multistep mechanism for ligand binding to WT with a differential temperature dependence of the individual steps.

Figure 5 illustrates the results of experiments in which the dissociation of GS−EA from the [GST·GS−EA] complex was investigated. Dissociation rate constants were obtained from the rate of the increase in intrinsic protein fluorescence after addition of 2 mM GSO_3^- to an equal volume of 2 μM GST equilibrated with 20−40 μM GS−EA. The trapping agent, GSO_3^-, like GSH, causes no change in the intrinsic fluorescence of GST, and thus, its binding is spectroscopically silent. The recovered rate constants for GS−EA dissociation were unchanged when the concentration of trapping agent was varied from 1 to 2 mM. Fluorescence data fit best to a double-exponential equation at temperatures

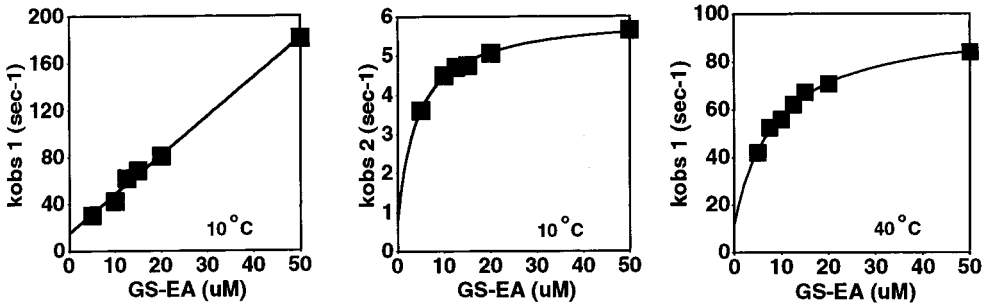

FIGURE 4: Dependence of the observed rate constants on GS−EA concentration at 10 and 40 °C. (Left) A linear relationship was established between k_{obs1} and [GS−EA] at 10 °C. The data were fit to the equation $k_{obs1} = k_{-1} + k_1$[GS−EA] ($R^2 = 0.96$). (Middle) A hyperbolic relationship was established between k_{obs2} and [GS−EA] at 10 °C. The data statistically fit better to a hyperbolic equation [$k_{obs2} = k_{-2} + k_2/(1 + K_1)$/[GS−EA]] than to a linear equation with R^2 values of 0.99 and 0.88, respectively. (Right) Dependence of the single observed rate constant, k_{obs}, on [GS−EA] at 40 °C. Statistically, the data fit better to a hyperbolic equation [$k_{obs} = k_{-2} + (k_2$[GS−EA])/([GS−EA] + K_1)] than to a linear equation with R^2 values of 0.99 and 0.79, respectively.

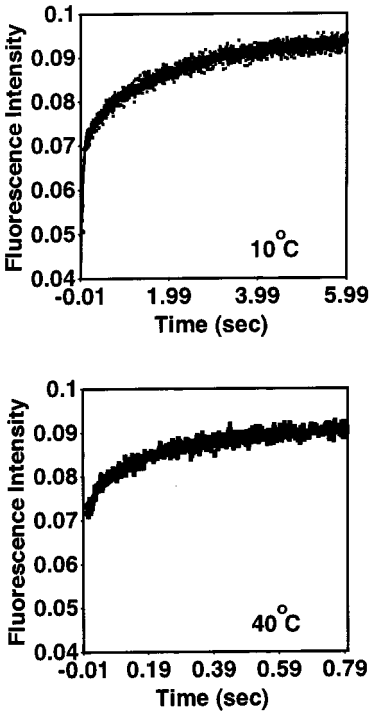

FIGURE 5: Kinetics of GS−EA dissociation from 2 μM [GST·GS−EA] complex at 10 (top) and 40 °C (bottom). (Top) Dissociation rates were determined directly from a double-exponential decay equation at 10 °C (R^2 = 0.97 and 0.76 for double- and single-exponential fits, respectively). (Bottom) The dissociation rate at 40 °C was determined from a single-exponential decay (R^2 = 0.94 and 0.96 for single- and double-exponential fits, respectively).

of ≤30 °C, yielding k_{-1} and k_{-2}, which correspond to fast and slow relaxation times, respectively. At 40 °C, a single dissociation rate was observed (Figure 5 and Tables 1 and 2). As observed in ligand binding experiments, the dissociation of GS−EA is complex at temperatures of <30 °C and multiple kinetic steps are apparent. An additional observation of some importance is that when two relaxation times are resolved for either binding or dissociation reactions, the slow event, k_2 and k_{-2}, is associated with a much larger pre-exponential term, suggesting that the magnitude of the fluorescence change due to this event is larger than that of the fast event, k_1 and k_{-1} (Tables 1 and 2). The observation of a biphasic process for ligand dissociation has significant implications for the population of enzyme forms present at equilibrium, as presented in the Discussion.

Δ209−222 Binding and Dissociation Kinetics. To determine whether the C-terminal helix contributes to either or both of the kinetic phases observed in the binding and dissociation experiments with WT, stopped-flow fluorescence experiments were performed with the Δ209−222 truncation mutant. In contrast to those of WT, the rates of ligand binding were too fast to measure above 20 °C and the magnitude of the total fluorescence intensity change was reduced to approximately 20% of the change observed with WT (Figure 6, left). Furthermore, a single relaxation time, k_{obs}, was observed, even at temperatures below 20 °C, at which the binding of ligand to WT was biphasic. Upon comparison of the observed binding rates, k_{obs}, to the narrow range of GS−EA concentrations which were used due to the rapidity of the reaction, a linear relationship was established. This suggests that WT and Δ209−222 rGST A1-1 have different binding mechanisms (Figure 6, middle). Fluorescence data for the dissociation of the ligand from the [Δ209−222·GS−EA] complex also fit well to a single-exponential decay at temperatures ranging from 10 to 40 °C (Figure 6, right, and Tables 1 and 2).

Equilibrium Binding Experiments. The equilibrium dissociation constant (K_d) of GS−EA for WT and Δ209−222 rGST A1-1 was experimentally measured by fluorescence titration at 25 °C. K_d values of 2.69 and 6.38 μM were determined by fitting the data to eq 2 for WT and Δ209−222, respectively. The maximum emission wavelength (λ_{max}) for Δ209−222 was red-shifted compared to that for WT (328 vs 325 nm), indicating that the presence of the C-terminus alters the environment of the single tryptophan (Trp-21), even though this residue is far away from the terminus. The fluorescence emission of both enzymes was red-shifted upon binding of GS−EA, indicating that an H-site ligand also alters the solvent environment of Trp 21, as suggested previously (*29*).

Analysis of Relaxation Data. Kinetic data were analyzed by comparison to five mechanisms (*30*−*34*). The bimolecular equation (eq I) is the simplest of all enzyme−substrate association reactions, in which the enzyme (E) and substrate (S) combine to form the final product (ES):

$$E + S \underset{k_{-1}}{\overset{k_1}{\rightleftharpoons}} ES \qquad (I)$$

Under pseudo-first-order conditions where [S] ≫ [E], k_{obs}

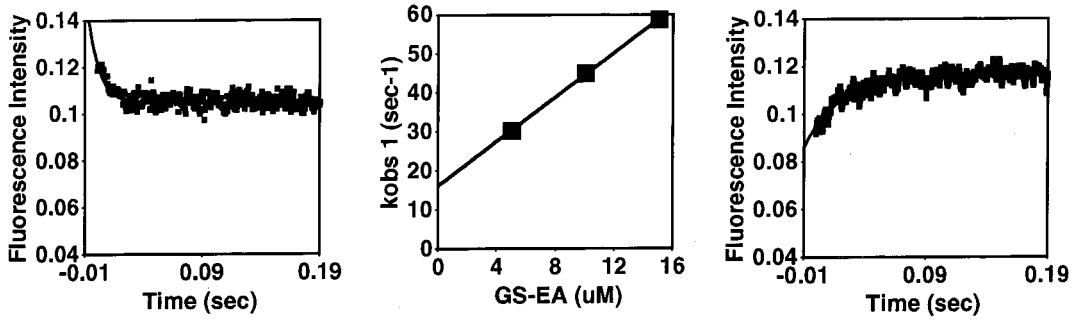

FIGURE 6: Kinetics of GS−EA binding and dissociation with Δ209−222 at 10 °C. (Left) Fluorescence data for the binding of 10 μM GS−EA to 1 μM Δ209−222 at 10 °C. The data fit best to a single-exponential equation (R^2 = 0.92). (Middle) Dependence of the observed rate constant on GS−EA concentration for Δ209−222 at 10 °C. Data were fit to a linear equation, yielding k_1 and $k_{-1(calc)}$ values of 2.86 × 10^6 M^{-1} s^{-1} and 16.1 s^{-1}, respectively. Only three rate constants were obtained because the reaction was too rapid to observe at higher GS−EA concentrations. (Right) Kinetics of GS−EA dissociation from the 2 μM [Δ209−222·GS−EA] complex at 10 °C. The dissociation rates were determined directly from a single-exponential decay fit, yielding a k_{-1} value of 20.4 s^{-1} (R^2 = 0.93).

Table 2: Steady-State and Microscopic Rate Constants at 10 °C[a]

	WT	Δ210−222
k_{cat} (s^{-1})	0.823	0.240
Amp_1[b]	0.00532	0.00458
Amp_{-1}[b]	0.00610	0.0263
k_1 (M^{-1} s^{-1})	3.04×10^6	2.86×10^6
$k_{-1(calc)}$ (s^{-1})[c]	12.9	16.1
k_{-1} (s^{-1})[d]	10.8	20.4
Amp_2[b]	0.0379	
Amp_{-2}[b]	0.0225	
k_2 (s^{-1})	4.97	
$k_{-2(calc)}$ (s^{-1})[c]	0.912	
k_{-2} (s^{-1})[d]	0.748	
$K_{d(exp)}$ (M)[e]	$(2.69 \pm 0.42) \times 10^{-6}$	$(6.38 \pm 0.9) \times 10^{-6}$
$K_{d(calc)}$ (M)[f]	0.658×10^{-6}	5.63×10^{-6}

[a] The standard deviations of each of the rate constants (k_1, k_{-1}, k_2, and k_{-2}) are given in the footnotes of Table 1. [b] Pre-exponential amplitude values as determined from single- and double-exponential decay equations. [c] Dissociation rate constants determined from the *y*-intercept of the k_{obs} plots shown in Figure 4. [d] Dissociation rate constants determined directly during stopped-flow experiments. [e] Equilibrium dissociation constant determined during titration experiments at 25 °C. [f] Equilibrium dissociation constant determined from the equation $K_{d(calc)} = k_{-1}/(k_1k_{-2})/(k_{-2} + k_2)$.

and k_1 are related in a linear manner:

$$k_{obs} = k_{-1} + k_1[S]$$

where [S] is the substate concentration and k_1 and k_{-1} are the forward and reverse reaction rates, respectively. In a plot of k_{obs} versus [S], the binding rate constant, k_1, is derived from the slope of the line and the dissociation rate constant, k_{-1}, from the *y*-intercept. Because this mechanism only accounts for the presence of one relaxation time, it is inconsistent with the observation of two relaxation rates for the WT enzyme. However, this scheme does satisfy the experimental observations for the binding and dissociation of GS−EA to Δ209−222. Rates for binding and dissociation of GS−EA to Δ209−222 [k_1 and $k_{-1(calc)}$] were therefore determined from the slope and *y*-intercept of the linear regression fit to the k_{obs} versus [GS−EA] plot, respectively (Figure 6, middle). The dissociation rate derived from the plot, $k_{-1(calc)}$, agreed well with the value determined directly in stopped-flow experiments, k_{-1} (Table 2).

The observation of two relaxation times for WT rGST A1-1 suggests that the enzyme acts by a mechanism that is more complex than that of Δ209−222. Therefore, four multistep schemes were considered. Mechanism II is a biexponential mechanism in which the formation of the final product, E*S, occurs in two steps:

$$S + E \underset{k_{-1}}{\overset{k_1}{\rightleftharpoons}} E^* + S \underset{k_{-2}}{\overset{k_2}{\rightleftharpoons}} E^*S \qquad \text{(II)}$$

As the enzyme slowly isomerizes between two conformations, E and E*, the substrate rapidly binds to one of these states to form the final product, E*S. At high substrate concentrations ([S] ≫ [E]), the two relaxation times for the isomerization and binding are related to substrate concentration in a nonlinear and linear manner, respectively:

$$k_{obs1} = k_1 + k_{-1}/[1 + ([S]/K_2)]$$

$$k_{obs2} = k_{-2} + k_2[S]$$

where k_{obs1} and k_{obs2} are related to the observed rates for the isomerization and binding steps of the reaction, respectively, and K_2 is equal to k_{-2}/k_2. Mechanism II predicts a linear relationship between k_{obs2} and [GS−EA] which increases with substrate concentration, in agreement with experimental data (Figure 4, left). However, this mechanism predicts an inverse relationship between k_{obs1} and [S], in which the observed rate decreases with increasing substrate concentration, in contrast to the experimental data (Figure 4, middle) (*32*−*35*). Because a hyperbolic dependence between k_{obs} and [GS−EA] is observed, this mechanism is not an appropriate model for WT rGST A1-1.

The third mechanism (eq III) that was considered is another two-step mechanism in which E and S rapidly combine to form the precomplex ES, which slowly isomerizes to a final complex, ES*:

$$E + S \underset{k_{-1}}{\overset{k_1}{\rightleftharpoons}} ES \underset{k_{-2}}{\overset{k_2}{\rightleftharpoons}} ES^* \qquad \text{(III)}$$

If it is assumed that the binding step, k_1, is significantly faster than the rearrangement, k_2, two relaxation times will be observed:

$$k_{obs1} = k_{-1} + k_1[S]$$

$$k_{obs2} = k_{-2} + k_2/[1 + (K_1/[S])]$$

k_{obs1} corresponds to the observed rate of the bimolecular association of E and S and k_{obs2} to the observed rate of the unimolecular isomerization between the two ES conformations.

This model predicts a linear plot of k_{obs1} versus [GS−EA], and a hyperbolic plot of k_{obs2} versus [GS−EA] which plateaus as k_{obs2} approaches $k_2 + k_{-2}$ (*32*−*35*). These predictions are in complete accordance with the experimental data (Figure 4, left and middle). Upon the experimental data being fitted to the above rate equations for model III, values for k_1 and k_2 were determined. In addition, dissociation rates, $k_{-1(calc)}$ and $k_{-2(calc)}$, determined from the *y*-intercept of each k_{obs} plot, were nearly identical to those determined experimentally, $k_{-1(exp)}$ and $k_{-2(exp)}$ (Table 2). Further verification of mechanism III is provided by the equilibrium binding data. The equilibrium dissociation constant, $K_{d(calc)}$, determined from fitting the experimental data to mechanism III was similar to the value measured directly in steady-state titration experiments, $K_{d(exp)}$, 0.658 and 2.69 μM, respectively.

The experimental observation of a single relaxation time at 40 °C does not disprove the occurrence of a multistep mechanism. Under some conditions, a single relaxation time may be observed even though the binding mechanism may be multistep in nature. When a single relaxation time is observed for an enzyme which behaves according to mechanism III, k_{obs} will be dependent on both the binding and isomerization steps of the reaction and is related to the substrate concentration by

$$k_{obs} = k_{-2} + [(k_2[S])/([S] + K_1)]$$

Under pseudo-first-order conditions, all of the enzyme is converted to the enzyme−substrate complex and the isomerization step of the mechanism dominates the reaction kinetics,

resulting in a hyperbolic k_{obs} plot, as is observed at 40 °C (Figure 4, right) (*36*).

Although model III provides a minimal kinetic mechanism consistent with the experimental data, the actual mechanism of rGST A1-1 may be more complicated. Additional steps which are present in the reaction may be kinetically silent because: (1) the relaxation times may be too fast to be detected by the instrument, (2) two relaxation times are very similar and cannot be distinguished, or (3) two different intermediates within the reaction mechanism have the same fluorescence quantum yields. These possibilities must be considered, especially in light of the dynamic nature of the C-terminus in the rGST A1-1 enzyme. Therefore, the experimental data were also compared to two additional multistep mechanisms to determine if the kinetic results exhibit characteristics of a more complicated model.

Mechanism IV is an extension of the two-step models where an isomerization step is included both before and after binding of the substrate; however, the substrate can only bind to one of the enzyme's conformational states:

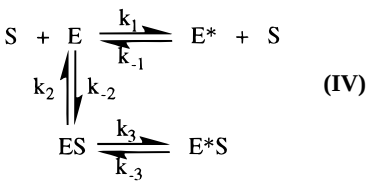

(IV)

If ligand binding is the most rapid step of the reaction and the conformational rearrangement after binding, k_3, is the slowest step of the reaction:

$$k_{obs3} = k_{-3} + k_3/\{1 + K_2/[[S]/(K_1 + 1)]\}$$

Expressions for k_{obs2} and k_{obs1} are identical to those found in mechanism II; they refer to identical steps in both mechanisms. According to the rate equations predicted by mechanism IV, the experimental data correspond well to k_{obs2} and k_{obs3}, as the mechanism predicts a direct linear relationship between k_{obs2} and [S], and a hyperbolic relationship between k_{obs3} and [S] (*32*, *33*). Therefore, for mechanism IV to apply to WT rGST A1-1, k_{obs1} must be kinetically silent. This would be true if E and E* have identical fluorescence characteristics. Upon our experimental data being fitted to this model, however, the calculated dissociation constant, $K_{d(calc)}$, is 0.5 M, much larger than the $K_{d(exp)}$ determined from titration experiments (2.69 μM). Therefore, mechanism IV, with the assumption that k_3 is the slowest step of the reaction, is inconsistent with our experimental data for rGST A1-1.

Conversely, if rearrangement before ligand binding, k_1, is slow, then:

$$k_{obs1} = k_{-1} + k_1/(1 + \{[S]/[(K_2K_3)/(1 + K_3)]\})$$

Relationships between k_{obs2} and k_{obs3} and [GS−EA] are obtained from the identical rate equations in mechanism III. Under this assumption, the k_{obs2} and k_{obs3} plots predicted by the mechanism are consistent with the two relaxation times observed experimentally, as indicated by the analysis for mechanism III. However, as discussed above, k_{obs1}, which should decrease with increasing substrate concentrations, must be kinetically silent, since a third relaxation time is not observed. We have no experimental or mathematical method for distinguishing this three-step binding mechanism (eq IV) from the simpler two-step mechanism (eq III) for WT rGST A1-1. Because the rate equations for k_{obs2} and k_{obs3} are identical to those in mechanism III, the same association rate constants and equilibrium dissociation constant are determined for both mechanisms (Table 2).

Mechanism V differs from scheme IV only in that ligand binding can take place on both the E* and E conformations:

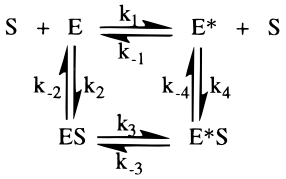

(V)

When binding is faster than isomerization, one relaxation time will relate to each of the binding steps, and the two conformational changes will be described by a single relaxation. Here, k_2, assumed to be the fastest binding rate, will be uncoupled from all events, and the observed rate, k_{obs2}, and [GS−EA] are related by a linear relationship:

$$k_{obs2} = k_{-2} + k_2[S]$$

The binding of substrate to the E* state is coupled to the fastest process by the common ligand, resulting in a second linear relationship:

$$k_{obs4} = k_{-4} + k_4[[S](K_2 + [S]/K_2 + [S])]$$

If this mechanism were appropriate for WT, the linear k_{obs} plot derived from our experimental data (Figure 4, left) could correspond to either k_2 or k_4. However, the third relaxation time predicted by this mechanism, which corresponds to the rearrangement steps, is not in agreement with the experimental data because as the substrate concentration is increased, the isomerization rates should decrease (*33*).

On the basis of the evaluation of these five mechanisms, our experimental results suggest that rGST A1-1 may act through either a two-step mechanism (eq III), in which E and S rapidly combine to form the precomplex ES, which slowly isomerizes to a final complex, ES*, or a three-step mechanism (eq IV), in which an isomerization step is included both before and after binding of the substrate, with the requirement that the substrate can only bind to one of the enzyme's conformational states. In contrast, in Δ209−222, only one relaxation time is observed, suggesting that the binding mechanism consists of a single reaction step. Notably, the recovered rate constants for binding and dissociation of GS−EA and Δ209−222 differ by less than 2-fold from the fast binding and dissociation components of the biphasic reaction observed for WT.

DISCUSSION

GST isoforms from each gene class have structural elements which define their catalytic properties and substrate selectivity. The C-terminal helix is a structural element that is unique to the A-class GSTs, and which defines its specificity and enzymatic activity. In X-ray crystal structures of the hGST A1-1 apoenzyme, the position of the C-terminus is undefined, unlike the ligand-bound structures, in which the C-terminus forms a helical cap over the active site (*16*,

17). Apparently, the conversion between the locally disordered and ordered state is a critical determinant of the enzymatic activity of GST A1-1.

Recently, kinetics of ligand binding have been studied for the P- and M-class GSTs. Cacurri et al. (*37*) determined a hyperbolic dependence between the observed rate of binding and GSH concentration in stopped-flow experiments, and suggested that the binding of GSH to the P1-1 enzyme may follow a two-step mechanism in which substrate binding is followed by a conformational change of the precomplex to the final Michaelis complex. In contrast, Parsons et al. (*38*) have determined that GSH or GSO_3^- binds to M1-1 GST at a rate that is slower than the limit of diffusion, and suggested that a rapid conformational change in the enzyme is necessary before the binding of substrate (*38*). Although a detailed analysis of ligand binding to the A-class GSTs has not been reported previously, our results indicate that it may also be complex. Interestingly, the dynamic nature of the C-terminus and its location in ligand-bound X-ray structures suggest that the C-terminus itself may control ligand binding to GST A1-1 (*16*, *17*).

Steady-state turnover rates of EA with WT rGST A1-1 in the presence of viscogen indicate that the rate-limiting step changes as the reaction temperature varies from 10 °C, where a physical step is rate-limiting, to 50 °C, where the chemical step is rate-limiting. Upon further analysis of this temperature dependence, the rates for dissociation of GS−EA from the [GST·GS−EA] complex correspond well to k_{cat} values at 10 and 25 °C (Table 1). This comparison illustrates that the physical step, which is at least partially rate-limiting between 10 and 40 °C, is product release. To determine whether the C-terminus affects the rate-limiting step of the conjugation reaction, rates of turnover of EA by Δ209−222 were also measured in the presence of viscogen. Interestingly, for this mutant, the chemical step is rate-limiting at all temperatures, providing evidence that the slow rate of product release in WT is due to the C-terminus.

Stopped-flow experiments established that the C-terminus also affects the binding of the ligand to the active site. Although the rates of the initial docking of GS−EA with WT and Δ209−222, k_1, are not significantly different, the WT enzyme exhibits a second, slow, relaxation process which is completely absent in Δ209−222 (Table 2). Upon comparison of five different kinetic mechanisms, WT A1-1 appears to act by one of two mechanisms: a two-step mechanism (eq III) in which an isomerization step occurs after ligand binding and a three-step mechanism (eq IV) in which the enzyme isomerizes both before and after the binding of ligand, but the ligand only binds to one state of the enzyme. For either mechanism, at least one conformational change must occur for the enzyme to reach its final equilibrium state. Because only a single relaxation time is observed in the Δ209−222 truncation mutant, we propose that the ligand-induced isomerization step in WT corresponds to the ordering of the C-terminus from a disordered to helical state.

As discussed above, the two mechanisms predicted for WT rGST A1-1 cannot be experimentally distinguished. However, structural and kinetic data suggest that the enzyme is less likely to act by mechanism IV than by mechanism III. If the enzyme has two conformational states in the absence of ligand, E and E*, structural differences between the two would most likely lie in the C-terminus; an obvious possibility is that the C-terminus fluctuates between a coil and a helix. This speculation is based on crystal structure data, in which the only significant difference between the apoenzyme and the GS−EA-bound hGST A1-1 lies in the C-terminus (*16*, *17*). Moreover, if the ordering of the C-terminus does result in a second isomer, E*, kinetic data suggest that these two conformational states would be spectrally distinguishable. Pre-exponential amplitude values from binding and dissociation experiments with WT suggest that approximately 20% of the GS−EA-dependent fluorescence change is due to the initial docking of GS−EA (k_1), while 80% is due to the isomerization step (k_2). In addition, in stopped-flow experiments with Δ209−222, in which the isomerization step presumably does not occur, the total fluorescence change is only about 20% of that of the WT binding reaction. These results suggest that the docking of GS−EA at the active site results in a small fluorescence change, while the isomerization provides a large change in protein fluorescence. Therefore, if a conformational change from E to E* involves the ordering of the C-terminus, as we predict for the transition of ES to ES*, the two conformational states should be able to be distinguished by their fluorescent properties, and detectable in kinetic binding experiments. Inasmuch as we do not detect an E* to E transition, we suggest that A1-1 is most likely acting by mechanism III and that a ligand-free form of GST with the helix intact is not present.

Mechanism III predicts that a single rate should be observed for the dissociation of GS−EA from the final [GST·GS−EA]* complex, because a slow disordering of the helix, k_{-2}, will mask the observation of the fast release of GS-EA, k_{-1}, from the intermediate [GST·GS−EA] complex. For mechanism III, however, a biphasic dissociation may be observed if a significant amount of the intermediate [GST·GS−EA] complex is present at equilibrium. Our results indicate that the observation of two distinct rates is likely due to the presence of this intermediate. The calculated K_2 value, determined from the ratio k_{-2}/k_2, indicates that approximately 15% of the total [GST·GS−EA] complex has a disordered helix at equilibrium. Therefore, it is likely that in our dissociation experiments, the displacement of GS−EA from the intermediate complex, [GST·GS−EA], results in the observation of the fast dissociation rate, k_{-1}, while the disordering of the helix in the final complex, [GST·GS−EA]*, results in k_{-2}. Kinetic simulations using the experimentally determined rate constants [k_1, $k_{-1(exp)}$, k_2, and $k_{-2(exp)}$] verify this interpretation and indicate that ∼15% of the intermediate will be present at equilibrium, even when experiments are performed with a 100-fold excess of GS−EA, where only 0.5% of the GST is ligand-free. At 40 °C, an identical K_2 value was calculated (not shown), suggesting that the coil−helix equilibrium with GS−EA bound is not temperature-dependent from 10 to 40 °C. Interestingly, the value of k_{-2} is more sensitive to temperature than k_{-1} in this range. This is consistent with the suggestion that k_{-2} reports on a nondiffusive step requiring protein motion. The presence of ∼15% of the [GST·GS−EA] intermediate containing a disordered helix at equilibrium is a result which is not immediately predicted from the X-ray structures. Obviously, the disordered state may include an ensemble of conformational states which cannot be resolved on the basis of our

experiments. In addition, it remains to be determined whether different GS conjugates afford differential fractions of the disordered state.

An additional consideration related to the observed kinetics is the conformational state of the ligand. Unbound GS−EA is expected to have a significant degree of conformational freedom. However, only a few members of the ensemble may approximate the conformation of the ligand within the active site of the enzyme. If interconversion between conformers of GS−EA were slow, this process could contribute of the observed binding kinetics. However, if the conformational dynamics of the ligand dominate the binding and dissociation kinetics, the slow relaxation time observed in experiments with WT would also be apparent in the Δ209−222 mutant.

In addition, we acknowledge that the ligand exists as a diastereomeric mixture. In principle, these diastereomers may bind to the enzyme at different rates, resulting in the observation of two relaxation times. Again, however, kinetic results with the Δ209−222 mutant demonstrate the presence of a single relaxation rate. Therefore, it is unlikely that the binding of different diastereomers to GST is directly responsible for the two relaxation times. Although the conformational dynamics and the stereochemical contraints of GS−EA may be an interesting aspect of the binding process, they are not addressed directly by these experiments.

Our studies demonstrate that the C-terminus controls rates of ligand association and dissociation for the rGST A1-1 enzyme. The results are easily rationalized in light of the available X-ray structures, which indicate the occurrence of ligand-dependent changes in the structure of the C-terminal helix (*16*, *17*). A surprising result of these studies, however, is the relative insensitivity of the equilibrium binding affinity (K_d) for GS−EA to the truncation of the C-terminus. The experimentally recovered K_ds for WT and Δ209−222 are 2.69 and 6.38 μM, respectively, which correspond to a $\Delta\Delta G°$ of 0.52 kcal/mol. Alternatively, if the recovered kinetic constants are used to calculate K_ds, then the $\Delta\Delta G°$ is 1.1 kcal/mol. This result suggests that the C-terminal helix contributes modestly to the stability of the ligand-bound complex. A similar conclusion has been reached for the ligand-free enzyme. On the basis of high-pressure fluorescence studies, a $\Delta\Delta G°$ for the coil−helix transition in the absence of ligand is ∼0.2−0.3 kcal/mol (*39*). The C-terminal strand also makes a contribution to stabilization of the transition state in the conjugation reaction with EA, inasmuch as the rate of the chemical step slows at least 3-fold and becomes rate-limiting upon removal of the C-terminal residues. Presumably, the C-terminal helix contributes to the binding of electrophilies to the H-site to form the ternary complex [GST·GSH·EA], as suggested by Board and Mannervik for GST A2-2, and to the transition state corresponding to the chemical step of the reaction (*19*).

Perhaps one of the most important results of these studies is the correlation of a specific rate constant with the coil−helix transition. As a result, it is now possible to monitor specifically these rate constants at variable temperatures with site-directed mutants, as probes of the transition state for this structural change. In addition, evidence for the presence of a persistent [GST·GS−EA] complex with a disordered helix suggests that GS conjugates do not cause the C-terminus to become a static "cap". It is likely that the equilibrium between disordered and helical states with ligand bound depends on the structure of the ligand, and the dynamics of the transition may vary with substrate.

ACKNOWLEDGMENT

The authors acknowledge David Baker (University of Washington) and members of his lab for the use and assistance in the operation of the BioLogic SFM4/QFM stopped-flow fluorimeter.

REFERENCES

1. Hayes, J. D., and Pulford, D. J. (1995) *Crit. Rev. Biochem. Mol. Biol. 30*, 445−600.
2. Bethane, K., Widersten, M., Engström, A., Kozarich, J. W., and Mannervik, B. (1994) *Proc. Natl. Acad. Sci. U.S.A. 91*, 1480−1484.
3. Tew, K. D. (1994) *Cancer Res. 54*, 4313−4320.
4. Müller, M., Meijer, C., Zaman, G. J. R., Borst, P., Scheper, R. J., Mulder, N. H., de Vries, E. G. E., and Jansen, P. L. M. (1994) *Proc. Natl. Acad. Sci. U.S.A. 91*, 13033−13037.
5. Mannervik, B. (1985) *Adv. Enzymol. Relat. Areas Mol. Biol. 57*, 357−417.
6. Meyer, D. J., Coles, B., Pemble, S. E., Gilmore, K. S., Fraser, G. M., and Ketterer, B. (1991) *Biochem. J. 274*, 409−414.
7. Pemble, S. E., Wardle, A. F., and Taylor, J. B. (1996) *Biochem. J. 319*, 749−754.
8. Armstrong, R. N. (1991) *Chem. Res. Toxicol. 4*, 131−139.
9. Graminski, G. F., Kubo, Y., and Armstrong, R. N. (1989) *Biochemistry 28*, 3562−3568.
10. Kong, K. H., Takasu, K., Inoue, H., and Takahashi, K. (1992) *Biochem. Biophys. Res. Commun. 184*, 194−197.
11. Dietze, E. C., Ibarra, C., Dabrowski, M. J., Bird, A., and Atkins, W. M. (1996) *Biochemistry 35*, 11938−11944.
12. Liu, S., Zhang, P., Ji, X., Johnson, W. W., Gilliland, G. L., and Armstrong, R. N. (1992) *J. Biol. Chem. 267*, 4296−4299.
13. Huskey, S. E., Huskey, W. P., and Lu, A. Y. H. (1991) *J. Am. Chem. Soc. 113*, 2282.
14. Liu, S., Ji, X., Gilliland, G. L., Stevens, W. J., and Armstrong, R. N. (1993) *J. Am. Chem. Soc. 115*, 7910−7911.
15. Mannervik, B., and Danielson, U. H. (1988) *CRC Crit. Rev. Biochem. 23*, 283−337.
16. Cameron, A., Sinning, I., L'Hermite, G., Olin, B., Board, P., Mannervik, B., and Jones, A. (1995) *Structure 3*, 717−727.
17. Sinning, I., Kleywegt, G., Cowan, S., Reinemer, P., Dirr, H., Huoer, R., Gilliland, G., Armstrong, R., Ji, X., Board, P., Olin, B., Mannervik, B., and Jones, T. (1993) *J. Mol. Biol. 232*, 192−212.
18. Nieslanik, B. S., and Atkins, W. M. (1998) *J. Am. Chem. Soc. 120*, 6651−6660.
19. Board, P. G., and Mannervik, B. (1991) *Biochem. J. 275*, 171−174.
20. Liu, L.-F., Liaw, Y.-C., and Tam, M. F. (1997) *Biochem. J. 327*, 593−600.
21. Ploemen, J. H. T. M., Van Schanke, A., Van Ommen, B., and Van Bladeren, P. J. (1994) *Cancer Res. 54*, 915−919.
22. Ploemen, J. H. T. M., Van Ommen, B., Bogards, J. J. P., and Van Bladeren, P. J. (1993) *Xenobiotica 23*, 913−923.
23. Awasthi, S., Srivastava, S., Ahmad, F., Ahmad, H., and Ansari, G. A. S. (1993) *Biochim. Biophys. Acta 1164*, 173−178.
24. Ploeman, J. H. T. M., Van Ommen, B., and Van Bladeren, P. J. (1990) *Biochem. Pharmacol. 40*, 1631−1635.
25. Dietze, E. C., Wang, R. W., Lu, A. Y. H., and Atkins, W. M. (1996) *Biochemistry 35*, 6745−6753.
26. Wang, R. W., Pickett, C. B., and Lu, A. Y. H. (1989) *Arch. Biochem. Biophys. 269*, 536−543.
27. Habig, W., Pabst, M., and Jakoby, W. (1974) *J. Biol. Chem. 249*, 7130−7140.
28. Kramers, H. A. (1940) *Physica (Amsterdam) 7*, 284−304.
29. Wang, R. W., Bird, A. W., Newton, D. J., Lu, A. Y. H., and Atkins, W. M. (1993) *Protein Sci. 2*, 2085−2094.

30. Eigen, M., and de Maeyer, L. C. (1963) in *Techniques of Organic Chemistry* (Weissberger, A., Ed.) Vol. 8, Part 2, p 895, Wiley, New York.
31. Eigen, M. (1967) in *Fast Reactions and Primary Processes in Chemical Kinetics* (Claesson, S., Ed.) p 333, Interscience, New York.
32. Eigen, M. (1968) *Q. Rev. Biophys. 1*, 3.
33. Halford, S. E. (1972) *Biochem. J. 126*, 727−738.
34. Fersht, A. (1985) *Enzyme Structure and Mechanism*, pp 121−154, Freeman, W. H., & Co., New York.
35. Halford, S. E. (1971) *Biochem. J. 125*, 319−327.
36. Quast, U., and Mählmann, H. (1982) *Biochem. Pharmacol. 31*, 2761−2768.
37. Cacurri, A. M., Lo Bello, M., Nuccetelli, M., Nicotra, M., Rossi, P., Antonini, G., Federici, G., and Ricci, G. (1998) *Biochemistry 37*, 3028−3034.
38. Parsons, J. F., Xiao, B., Gilliland, G. L., and Armstrong, R. N. (1998) *Biochemistry 37*, 6286−6294.
39. Atkins, W. M., Dietze, E. C., and Ibarra, C. (1997) *Protein Sci. 6*, 873−881.

BI9829130